MATERIALS SCIENCE

Stoichiometric control of the density of states in PbS colloidal quantum dot solids

Daniel M. Balazs,[1] Klaas I. Bijlsma,[1] Hong-Hua Fang,[1] Dmitry N. Dirin,[2,3] Max Döbeli,[4] Maksym V. Kovalenko,[2,3] Maria A. Loi[1]*

Colloidal quantum dots, and nanostructured semiconductors in general, carry the promise of overcoming the limitations of classical materials in chemical and physical properties and in processability. However, sufficient control of electronic properties, such as carrier concentration and carrier mobility, has not been achieved until now, limiting their application. In bulk semiconductors, modifications of electronic properties are obtained by alloying or doping, an approach that is not viable for structures in which the surface is dominant. The electronic properties of PbS colloidal quantum dot films are fine-tuned by adjusting their stoichiometry, using the large surface area of the nanoscale building blocks. We achieve an improvement of more than two orders of magnitude in the hole mobility, from below 10^{-3} to above 0.1 $cm^2/V \cdot s$, by substituting the iodide ligands with sulfide while keeping the electron mobility stable (~1 $cm^2/V \cdot s$). This approach is not possible in bulk semiconductors, and the developed method will likely contribute to the improvement of solar cell efficiencies through better carrier extraction and to the realization of complex (opto) electronic devices.

INTRODUCTION

Colloidal quantum dot (CQD) solids have attracted much attention in the past two decades because of their physical properties, yielding great potential for application. Their solution processability, coupled with high absorption and crystalline robustness, allows for the fabrication of efficient solar cells and photodetectors (*1*, *2*), whereas the tailorable electronic structure through size and interdot coupling opens a way to novel physical phenomena and unprecedented combination of properties (*3*–*5*). Recently, the first transistors fully based on colloidal materials were reported (*6*). Despite the promises, full control of the electronic structure has not been achieved, because most lead-based, supposedly intrinsic samples predominantly show dominant n-type conductivity (*7*–*9*) and efficient p-type transport is only achieved upon air exposure (*1*, *10*, *11*). The lack of high-quality p-type layers has recently been identified as one of the limiting factors for the solar cell performance (*12*).

In bulk inorganic semiconductors, the carrier density control is usually achieved by doping—inserting aliovalent (usually hetero-) atoms in the lattice that introduce donor or acceptor states in the bandgap. However, this approach cannot be used in colloidal semiconductors because of their small size. The lattice strain stemming from the incorporation of a heteroatom can be easily resolved by diffusion toward the surface and formation of dopant clusters ("self-purification"), or synthesis is not possible (*13*). It has been described that off-stoichiometry in compound semiconductors can cause carrier imbalance, because the valence and conduction band states have different "origin" (for example, dominant S 3p and Pb 6p orbitals in PbS, respectively); thus, uncompensated states will reside near either the conduction or the valence band (*14*). Kim *et al.* (*15*) calculated that quantum dots with excess lead on their surface show n-type characteristics due to filled midgap states present near the conduction band. This off-stoichiometry is typical of all colloidal lead chalcogenide samples because the lead oleate shell provides colloidal stability. Moreover, it is also predicted that this situation can be inverted, turning them to p-type, by (over)compensating the initial off-stoichiometry. According to the calculations of Kim *et al.*, thiol ligands attached to the surface can also compensate the off-stoichiometry, but the covalently bound sulfur only contributes one-half to the effective stoichiometry, limiting the possibility of compensating for the initial unbalance.

Oh *et al.* showed experimentally that ligand exchange with chalcogenide salts can result in strong p-type CQD solids (*16*) and that modification of the charge carrier concentration is possible by thermal evaporation of either elemental lead or chalcogens on top of the film (*17*). Stavrinadis *et al.* reported sulfurization of PbS particles by exposing the as-deposited thin films to an organosulfur compound (*18*). Although these works are groundbreaking and provide proof-of-concept results, all of the described methods have drawbacks; either only full surface coverage with the chalcogen can be realized or the stoichiometry is inhomogeneous throughout the film. A direct approach that provides reliable, fine control of the transport properties and the electronic structure by changing the layer stoichiometry has not been achieved. Moreover, the exact mechanism of the reported changes is generally not understood.

Here, we propose a strategy to enhance the p-type conductivity of PbS CQD solids by modifying the lead-to-sulfur ratio using a fully solution-based and low-temperature method. A two-step ligand exchange based on the different affinity of sulfide and iodide to the surface of the Pb chalcogenides is used to control the surface composition. We demonstrate that this method is suitable for fine control of stoichiometry and for boosting hole mobility while barely affecting electron transport, indicating significant changes in electronic structure. This facile engineering of electronic properties is unique to CQD solids, and demonstrates the potential of these materials for the field of solution-processed semiconductors. The developed method could be the next step toward the long-sought confined-but-connected quantum dot solids and novel devices based on them.

RESULTS

Layers of 3.5-nm PbS particles were formed by spin-coating on solid substrates, following the procedure described in Materials and Methods. The excess sulfur is introduced as anhydrous sodium bisulfide (NaHS)

[1]Zernike Institute for Advanced Materials, University of Groningen, Nijenborgh 4, Groningen 9747AG, Netherlands. [2]Department of Chemistry and Applied Biosciences, ETH Zürich, Vladimir Prelog Weg 1, Zürich 8093, Switzerland. [3]Swiss Federal Laboratories for Materials Science and Technology (Empa), Überlandstrasse 129, Dübendorf 8600, Switzerland. [4]Laboratory of Ion Beam Physics, ETH Zürich, Otto-Stern-Weg 5, CH-8093 Zürich, Switzerland.
*Corresponding author. Email: m.a.loi@rug.nl

dissolved in methanol. Other compounds, such as K_2S, Na_2S, $(NH_4)_2S$, and solvents (isopropanol, ethanol, and water), have also been studied and lead to similar results, but their limited solubility and the formation of the conjugate base of the solvent make the experiments less reproducible. Generally, strong cracking and almost complete delamination are observed when thick PbS films are directly exposed to a solution with high sulfide concentration, indicating a rapid reaction that causes reorganization. The effect is much stronger than when thiols, amines, or halides are used. This strong reaction can be rationalized by the high lattice formation energy of PbS. The (bi)sulfide ions have a larger affinity to the surface of the quantum dots than any other ligands. To limit the effect of the reaction, we developed a two-step exchange, which results in homogeneous and crack-free layers (Fig. 1A). Using iodide ligands in the first step, a large amount of oleic acid can be removed, and the CQDs reorganize gently without disrupting film quality. The stoichiometry is altered in the second step by exposing the films to the sulfide solution, which is expected to (partially) replace the initially formed iodide shell. The amount of introduced sulfur is controlled by applying the same volume of solutions with different concentrations.

To shed light into possible structural transformations that may occur during the process, we investigated the structure of the layers after the two-step treatment. Figure 1 shows transmission electron microscopy (TEM) micrographs collected from submonolayer films treated with iodide only (Fig. 1, B and C) and with a subsequent exposure to high (millimolar) concentrations of sulfide solution (Fig. 1, D and E). The particle shape and size remain intact upon treatment with sulfide, and all the samples show the square superlattice ordering that has been observed in many lead chalcogenide samples treated with halides (*9*, *16*, *19*). The typical lattice spacing (4.2 nm) determined from the Fourier-transformed images (insets of Fig. 1) is identical in the samples before and after the sulfide treatment. This is larger than the 3.5-nm particle size calculated from the solution-phase absorption measurement (fig. S1) (*20*). The increase in spacing is assigned to necking by migration of ions into the gap between adjacent particles (*9*). A more pronounced neck formation is found in the sulfide-treated samples (Fig. 1E), with increased number of superlattice defects and dislocations. These observations suggest that the epitaxial fusion is promoted by exposure to sulfide, even after an initial sulfide-free ligand exchange. In agreement with the high reactivity of the sulfide solution with PbS CQDs, this treatment leaves less time and opportunity for the particles to rearrange.

The optical properties of the films also vary with sulfide treatment (Fig. 2, A and B). The absorbance spectra of samples without sulfide treatment (Fig. 2A) show strong excitonic features, and the particles retain their confinement upon mild (120°C) annealing, with only minor broadening. However, the sulfide treatment weakens this resistance such that the absorption feature becomes less pronounced when samples prepared with 100 μM NaHS solution are annealed. Furthermore, the excitonic peak disappears completely at concentrations above 200 μM (even without annealing). The photoluminescence (PL) peaks of the same samples shift toward lower energies with increasing sulfide concentrations (Fig. 2B), whereas their peak intensity decreases by a factor of 3. A Gaussian fit of the measured PL data allows us to extract peak positions that correlate with the optical bandgap in these systems. The fitted energies are 0.93, 0.85, and 0.54 eV for samples treated with 0, 100, and 300 μM sulfide concentrations, respectively (fig. S2). Adjacent particles that merge with a broader neck express a lower confinement for charge carriers, resulting in a decreased bandgap or in almost bulk properties in the extreme case. However, even the sample with the lowest emission energy retains part of the quantum confinement, as the room temperature bulk bandgap of PbS is about 0.41 eV (*21*).

To understand the changes in the properties and confirm the effect of the treatments, we determined the film elemental composition

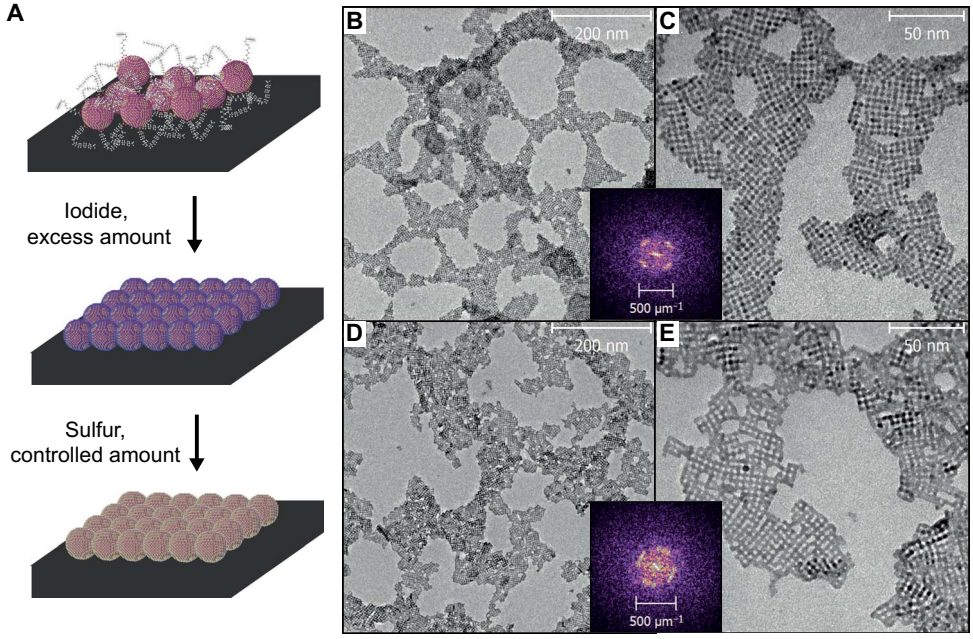

Fig. 1. Two-step treatment for ligand exchange and stoichiometric control and the related structural changes. (**A**) Schematics of the treatment: The initial exposure to the iodide solution removes oleic acid, and the sulfide treatment modifies the stoichiometry. (**B** and **C**) TEMs of an iodide-only sample at different magnifications, showing a square superlattice. (**D** and **E**) Similar structure of a sample treated with excess sulfide. (Insets) Fourier-transformed images taken from single superlattice domains of the two samples.

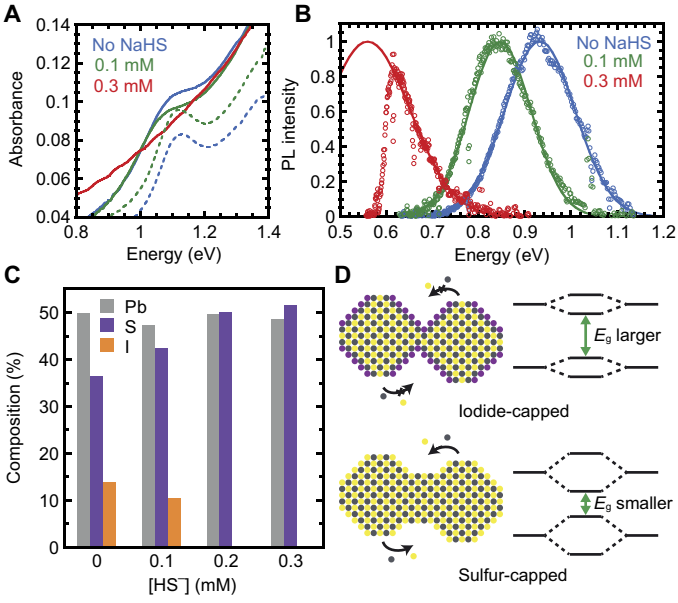

Fig. 2. Optical properties and composition of the sample with various stoichiometries. (**A**) UV-vis absorption spectra of films prepared with various sulfide concentrations before (dashed lines) and after (solid lines) annealing at 120°C. (**B**) PL spectra of annealed samples prepared with the same concentrations: measured data (markers) and Gaussian fit (lines). The peak of the sample treated with 0.3 mM NaHS extends below the detector cutoff. (**C**) Stoichiometry of films determined using Rutherford backscattering spectrometry (RBS): A trend from lead-rich to sulfur-rich is observed in the samples treated with different amounts of NaHS. (**D**) Model explaining the enhanced necking in sulfur-rich samples and the resulting decreased bandgap due to loss of quantum confinement.

using RBS. The measured spectra are shown in fig. S3. Other methods, such as x-ray photoelectron spectroscopy and energy-dispersive x-ray spectroscopy, were also tested but were found to be unsuitable for elemental quantification in our samples. The reference films (with no added sulfur) show a large excess of lead and 14% iodine (Fig. 2C). As the sulfide concentration increases, the iodide content decreases and drops to trace levels for samples treated with 200 μM NaHS. The sulfur content shows an opposite, increasing trend, confirming that the added sulfur predominantly replaces the iodine at the CQD surface. The sample treated with 200 μM sulfide is close to stoichiometric; further increasing the concentration turns the material sulfur-rich (Fig. 2C).

By correlating the changes in the spectra and the film stoichiometry, we observe that the disappearance of the excitonic feature and the strong red shift coincides with the compensation of the initial excess of lead and the disappearance of iodine. During the exchange from iodide to sulfide, the particles partially merge, decreasing the quantum confinement, as seen from the PL peak shift (see also Fig. 2D). The findings demonstrate that the iodide-capped surfaces are rather stable and prevent surface diffusion to the necking points, thus retaining the quantum confinement. The excess sulfur, on the other hand, gives higher surface ion diffusivity or has preferential filling to the gaps, resulting in broader necks (Figs. 1D and 2D).

Using these data, we make an attempt to calculate the number of sulfur atoms involved in these processes (see the details in the Supplementary Materials). On the basis of the film geometry and the nominal solution concentration, we estimate that 475 ± 15 sulfur atoms per CQD are added when using 200 μM NaHS. This value seems oddly high given that the total number of atoms in each QD, based on its diameter, is around 870 ± 40. However, on the basis of the RBS results, the number of iodine atoms is estimated to be 140 ± 10 per CQD, and the same 140 ± 20 sulfur atoms per CQD are added to achieve stoichiometry, whereas only 25 sulfurs per dot are added using the 300 μM solution. Therefore, these data suggest that the number of sulfur atoms that can bind to a CQD is limited and tends to saturate. The amount of sulfur introduced differs from the measured one by a factor of ~4. We observe that films treated with sulfides are thinner than the iodide-only ones, likely caused by a loss of particles and delamination. This latent amount, together with incomplete reaction, can be accounted for the sulfur loss.

To test the effect of stoichiometric variation on the electronic structure and transport properties, we fabricated field-effect transistors (FETs) using silicon oxide as the bottom gate electrode to modulate the current. The reference device (no sulfide added) shows the usual asymmetric, electron-dominated transport, with linear mobilities of 0.1 $cm^2/V \cdot s$ and 3×10^{-4} $cm^2/V \cdot s$ for electrons and holes, respectively. Adding sulfur initially increases both electron and hole currents, then suppresses the electron, but further increases the hole conductivity (Fig. 3, A and B). The conductivity in devices treated with >150 μM NaHS cannot be efficiently modulated. The corresponding output curves in Fig. 3C lack the linear and saturation regimes expected for semiconductors. However, the material does not behave as a metal either, the output curves are not linear, and a slight change in the conductivity is observed upon application of high gate voltages. The directions of the changes suggest the dominance of carriers with positive charge (holes). Similar findings were reported by Oh *et al.* (*16*) and explained by heavy p-doping of the semiconductor.

Our FETs can be made operational at temperatures below 200 K (Fig. 3, D and E), and gate-controlled conductivity spanning almost five orders of magnitudes is observed when the temperature is further lowered. A resistive, "off" state region appears at high positive gate voltages; the observed characteristics match those of a p-type doped semiconductor. The off current (defined as the value measured at V_G = +70 V) increases sharply in a supralinear manner with temperature (Fig. 3F). The high-temperature behavior of the off current can be fit with an Arrhenius-like equation, $A^*\exp(-E_a/k_BT)$, giving an activation energy $E_a \approx 0.2$ eV (fig. S4).

In the presence of acceptor states above the valence band, which may be filled by thermal activation, the charge carrier concentration can change significantly with temperature. However, the "carrier freeze-out" usually happens at much lower temperatures than observed here, indicating deep states in the middle of the bandgap and contradicting the initial assumption. These deep states would trap charge carriers and also cause a strong temperature dependence of the "on" state conductivity in the low-temperature regime, which is not observed in Fig. 3F. The intrinsic carrier concentration in a crystalline semiconductor at high temperatures scales with $\exp(-E_g/2k_BT)$, where E_g is the bandgap of the material. The activation energy significantly decreases in the presence of energetic disorder (decreased effective bandgap). The low bandgap and the disorder observed in the spectroscopy data (blurred excitonic peak absorption and red-shifted emission using high sulfide concentration) can give rise to such a temperature dependence ($2^*E_a = 0.4$ eV, from the off currents, versus $E_{g,PL} = 0.54$ eV, from the red curve in Fig. 2B).

The high number of charge carriers sets boundaries for the operability of a transistor; the accumulated charges in the channel have an upper limit, defined by the gate capacitance and breakdown voltage. Being unable to modulate the current in some devices suggests that we

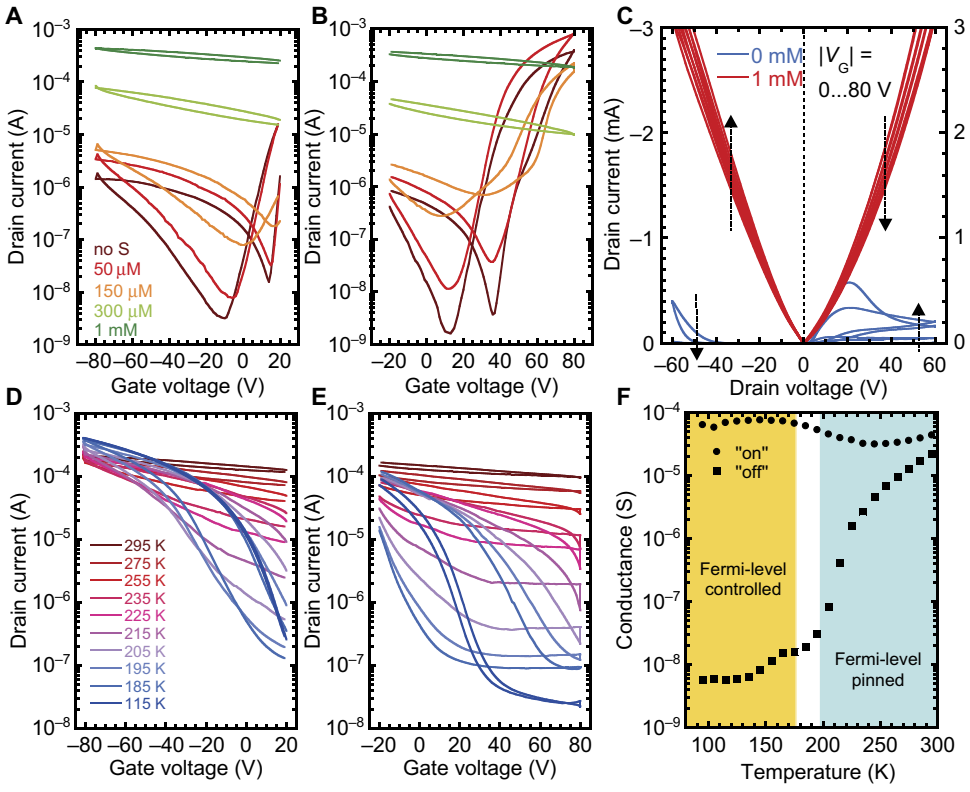

Fig. 3. Transport properties measured in SiO_2-gated FETs. P-channel (**A**) and n-channel (**B**) transfer curves of SiO_2-gated thin-film transistors prepared by varying the semiconductor stoichiometry. (**C**) Output characteristics of selected devices. Arrows indicate how the curves change, by applying higher positive (right side, n-channel) or higher negative (left side, p-channel) gate biases. (**D** and **E**) Transfer characteristics of a sulfur-rich device (10 mM, NaHS) measured at different temperatures at ±5-V bias, showing the presence of p-type (D) and the lack of n-type (E) characteristics. (**F**) On and off state conductivities as functions of the temperature, extracted from the data in (C) and (D) at V_G = −70 V and +70 V, respectively.

need a gate with significantly higher performance. With ionic liquids as gate dielectric, heavily doped materials can be turned ambipolar (*22*), insulating, metallic (*23*), and even superconductive (*24*). It has also been demonstrated that by using these electrolyte gates, traps can be filled (improving charge carrier mobility) (*25*, *26*), the bandgap can be determined from the electron and hole threshold differences (*27*, *28*), and the influence of heteroatom doping in CQD solids can be shown (*29*). In a typical electrolyte-gated transistor, charge carriers in the order of 10^{14} to 10^{15} cm^{-2} can be accumulated, whereas the SiO_2 gate used in the previous experiment is capable of accumulating 10 to 1000 times less carriers. A robust way to use ionic liquids is by forming ion gels, stabilizing the ionic liquid in a polymer matrix (*30*).

By using 1-ethyl-3-methylimidazolium bis(trifluoromethylsulfonyl) imide (EMIM TFSI) ionic liquid dispersed in a matrix of polyvinylidene difluoride–hexafluoropropylene (PVDF-HFP) copolymer as gate dielectric (see Fig. 4A for measurement setup and device structure), we manage to control the charge carrier density and measure the transport properties in every sample. The transfer curves measured at extremely low bias (0.1 V) are shown in Fig. 4B. We observe an increase in the hole current with the sulfide concentration up to 200 µM; this value agrees with the amount of sulfur required for stoichiometric composition based on the RBS results (see Fig. 2C). The minimum (off) current also increases more than three orders of magnitudes, and the position of the off state slightly shifts toward higher positive voltages with an increasing amount of sulfide. Above the 200 µM concentration, the hole current does not increase further, but the whole curve is shifted toward higher voltages, and electron accumulation becomes more difficult to observe because of the electrochemical limits of the ionic gel CQD system (*28*). However, by collecting data from several samples, it is possible to qualitatively describe both the electron and hole transport properties. The effect of a possible injection barrier was ruled out by determining the conductivity of films on glass substrates using a linear four-point probe method; the values show an increase similar to that of the off state currents (fig. S5).

The field-effect mobility (µ) and threshold voltage (V_{th}) values were obtained from the linear regime transfer curves based on the gradual channel approximation (Fig. 4, C and D). By adding sulfide, we observe a hole mobility increase of two to three orders of magnitude compared to that in the iodide only–treated PbS CQDs, whereas the electron mobility shows only minor variation. The hole mobilities achieved are the highest in fully inorganic PbS FETs (table S3) and comparable to the thiol-treated ones, with improved on/off ratio in the p-channel. The threshold voltages show a roughly linear dependence on the sulfur concentration for both electrons and holes, with higher slope in the latter case. It has been shown that the threshold voltage in ion gel–gated transistors describes the actual Fermi-level shift needed to accumulate the chosen charge carrier, providing a good estimate of the relative band edge energies (*28*). Consequently, the observed threshold trends indicate a gradual change in the position of the band edge or Fermi energy levels with increasing sulfide concentration, indicating a more p-type material and a parallel decrease in the electronic bandgap (in agreement with the red-shifted PL spectra) (*31*).

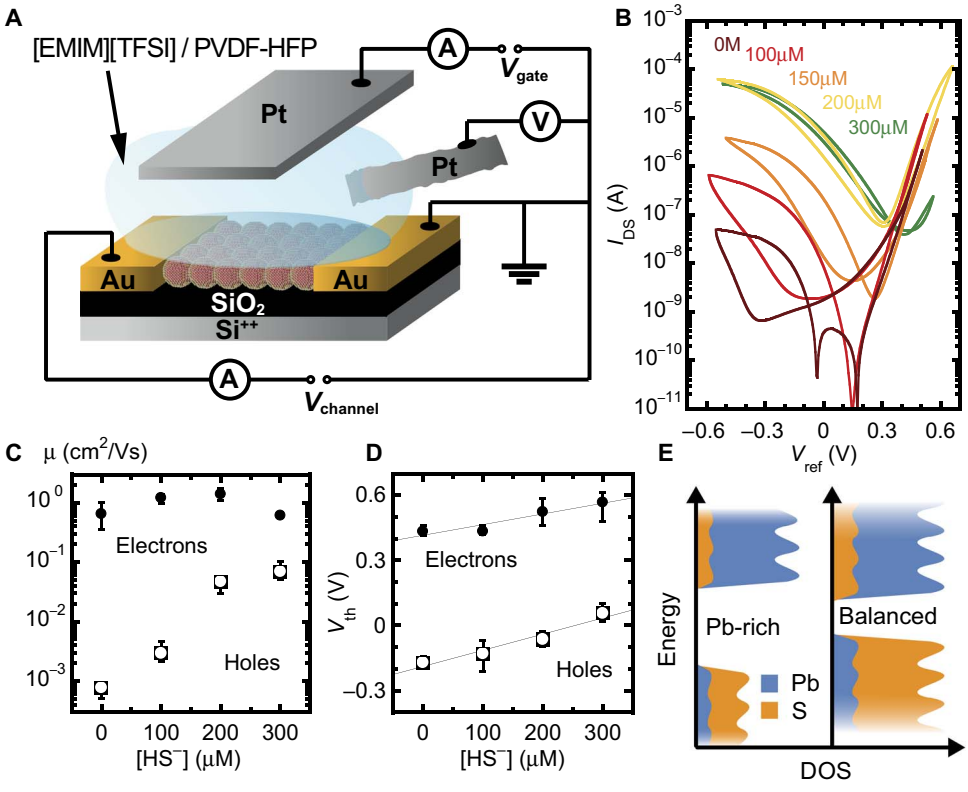

Fig. 4. Device structure and behavior of the ion gel–gated FETs. (**A**) Schematic of the device structure and the measurement circuit. (**B**) Transfer curves of devices prepared with various sulfide concentrations. Mobility values (**C**) and threshold voltages (**D**) obtained from several devices, showing the full range spanned by the single data points. (**E**) Schematics of the variation in the DOS: The sulfur contributes predominantly to the state density in the valence band.

DISCUSSION

Halide- and pseudohalide-capped PbS CQDs, when used in transistors, usually give asymmetric, electron-dominated ambipolar (or even unipolar n-type) current (*7*–*9*). Because the properties (effective mass, degeneracy, and measured mobility) of band edge electrons and holes are fairly similar in close-to-stoichiometric bulk PbS (*14*, *32*), one can expect balanced electron and hole transport in the stoichiometric but quantum-confined case as well. We observe this behavior in Fig. 4B (yellow curve), measured in a close-to-stoichiometric film, whereas the curves with <200 μM NaHS show the usual asymmetry to a different extent.

We identify the electronic structure of the material as the cause of the variation of the current-voltage characteristics. In PbS bulk and nanocrystals, the valence and conduction band states have distinctly different compositions. In the linear combination of atomic orbital interpretation, the valence band states are dominated by 3p orbitals of the S atoms, whereas the conduction band states consist mainly of 6p states of the Pb atoms (*15*). If the numbers of orbitals that contribute to the conduction and valence bands are different, the band structure becomes asymmetric, causing different bandwidth/density of states (DOS) for valence and conduction bands. Consequently, the frequently observed mobility difference between electrons and holes can be attributed to the off-stoichiometric electronic structure (Fig. 4E) (*15*). Considering that the addition of sulfur atoms to the particles increases the number of atomic orbitals that participate in the formation of the valence band edge states, a higher valence bandwidth/DOS is expected for samples with compensated stoichiometry, providing higher transfer integral and lower interdot resistance specifically for holes. We observe this exact phenomenon in the mobility plot in Fig. 4C; the hole mobility increases as a result of the treatment, whereas the electron mobility remains in the same range.

Although the observed behavior of both the low-temperature and ion gel–gated transistors match that of the p-type material, the band structure change cannot be accounted for the shift of the off state of the transfer curves and the threshold voltages. In ambipolar transistors, the device is in the off state when the Fermi level at the semiconductor-dielectric interface (in the channel) is shifted close to the middle of the bandgap (thus, the DOS around the Fermi level is practically zero) by applying an external gate potential. A shift in the measured threshold values will then indicate a different initial Fermi-level position relative to the band edges or a different position of the whole band structure versus the platinum work function. The former is a clear sign of altered charge carrier balance and actual doping in bulk semiconductors, whereas the latter is a common feature in semiconductor nanocrystals in the presence of surface dipoles (*33*). Considering the electronic configuration of the ions in the quantum dot, the addition of a closed-shell sulfide ion should not decrease the valence band filling and should not cause doping. The electron counting methods described by Kim *et al.* (*15*) or Voznyy *et al.* (*34*) give no overall change in the doping if doubly ionized lead or sulfur is added. From this perspective, a sulfide or bisulfide is isoelectronic to the original capping iodide ion. Consequently, the change of the stoichiometry with (bi)sulfide ions should cause only electronic structure changes and no real doping, and the observed threshold shifts are likely caused by surface dipoles of different binding geometries of the sulfide ions. Although it is not doping in a classical sense, the resulting effective p-type behavior leads

to improved charge carrier extraction and increased efficiency in PbS CQD solar cells, showing the prospects of the method (*35*).

In conclusion, we successfully achieved control of the stoichiometry of PbS CQD films through a two-step ligand exchange. The first step with iodide provides full removal of the oleic acid, and the second step with hydrogen sulfide ions adjusts the stoichiometry up to the point where the film turns sulfur-rich. The variation of the lead-to-sulfur ratio results in fine-tunable changes in the transport properties of the CQD films; the initially asymmetric, electron-dominated transport is turned into balanced ambipolar while compensating for the initial excess lead. In the figure of merits, the hole mobility increases the order of magnitude up to 0.1 $cm^2/V \cdot s$, whereas the electron mobility remains around 1 $cm^2/V \cdot s$. We explain the increased mobility using a significantly changed electronic structure, with the increase of the DOS specifically of the valence band. It is important to note that electronic structure engineering to such extent is not possible in bulk materials but is possible in nanostructures because of the emerging high surface area. The method used for sample fabrication is proven useful in tailoring the properties of strongly coupled CQD arrays, adding a new item to the researchers' toolbox and opening new application possibilities for CQD assemblies.

MATERIALS AND METHODS

Synthesis of PbS CQDs

PbS CQDs were synthesized according to the method of Hines and Scholes (*36*), with slight modifications. $Pb(CH_3COO)_2 \times 3H_2O$ (1.5 g), 1-octadecene (ODE) (47 ml), and oleic acid (3.2 ml) were mixed in a three-neck flask. The mixture was degassed under vacuum at 120°C for 1 hour and heated to 140°C under argon flow. The heating mantle was removed, and the solution of bis(trimethylsilyl) sulfide (0.42 ml) in 10-ml dried ODE was injected into vigorously stirred lead oleate solution at 140°C. After 5 min, the reaction mixture was cooled down to room temperature. The CQD were washed three times with toluene/ethanol solvent/nonsolvent pair, redissolved in hexane, and filtered through a 0.2-μm polytetrafluoroethylene filter.

Film formation and ligand exchange

All solvents were purchased from Sigma-Aldrich and were anhydrous, except for substrate cleaning. Substrates were cleaned before sample fabrication by sonicating in acetone and isopropanol. With the exception of the transistor fabrication, the substrates were pretreated with (3-mercaptopropyl)trimethoxysilane (MPTMS, 95%; Sigma-Aldrich) dissolved in toluene at 0.1 M for 1 hour and then washed with isopropanol. Thin films (~6 nm) of PbS CQDs dispersed in hexanes were formed by spin-coating. The films were flooded with a 20 mM solution of formamidine hydroiodide (TCI Chemicals, >98%) in methanol for 20 s, and the liquid was then removed by spinning the substrate. A controlled amount of a sodium bisulfide (NaHS, Alfa Aesar, anhydrous) solution was rapidly dropped on the substrate using an automatic pipette. The amount of liquid was determined by the substrate size (linearly scaled, 33 $\mu l/cm^2$). After 15 s, the liquid was spun off and the substrate was washed with methanol. The deposition was repeated 4 times for transport and absorption measurements and 10 times for PL and RBS samples. The samples were annealed at 120°C for 20 min.

Film characterization

TEM samples were prepared by drop-casting the solutions in the same order and amount (as specified previously) on MPTMS-treated SiO_2/Si membranes (SiMPore). The samples were characterized using a JEOL 2010 microscope. The samples for RBS were prepared on MPTMS-treated silicon wafers using the method described earlier. The composition was determined by 4-MeV He RBS at the ETH Laboratory of Ion Beam Physics using a silicon PIN diode detector under 168°. The relatively high energy of the beam used for the analysis allowed the separation of all the peaks of the relevant elements. The data were analyzed with the RUMP software to obtain the stoichiometry (*37*).

Ultraviolet-visible (UV-vis) absorption spectra were measured on glass substrates using a Shimadzu UV-3000 spectrometer. The PL measurements were performed using the second harmonic (400 nm) of a Ti:sapphire laser (repetition rate, 76 MHz; Mira 900, Coherent) to excite the samples. The illumination power density was decreased to 5 $\mu J/cm^2$ by a neutral density filter. A spectrometer and a cooled array detector (iDus InGaAs, 2.2 μm; Andor) were used to record the spectra. The PL measurements were performed on films on quartz substrates in a nitrogen-filled sample holder at room temperature.

Transport measurements

The samples were prepared on pieces of SiO_2/Si wafers that were used as the bottom gate electrode. No MPTMS was used, but each PbS layer was annealed for 2 min to avoid delamination. The 1-cm-wide and 20- or 2.5-μm-long channels (for SiO_2 and ion gel–gated measurements) were patterned by lithography and consisted of 10-nm indium tin oxide (ITO) and 30-nm gold.

The ion gel for the top gate was prepared by dissolving EMIM TFSI (>97%; Sigma-Aldrich) and PVDF-HFP (Sigma-Aldrich) in cyclohexanone at a 4:1:7 weight ratio (*38*). The mixture was homogenized at 70°C, dropped on the device areas, and dried at 70°C overnight in a glove box. Platinum foil was placed on top of the dry droplet as a gate contact, and a freshly cut Pt wire was inserted to measure the reference potential. The transfer curves were obtained at low (0.1 V) drain-source bias, and the gate potential was scanned at a rate of 10 mV/s within the electrochemical window of the electrolyte. Characterization of the ion gel capacitance is presented in the Supplementary Materials. All room temperature transport measurements were performed in a nitrogen-filled glove box. The semiconductor parameter analyzers used in this work are the following: Agilent E5262A for SiO_2-gated transistors, Keithley 4200-SCS for the electrolyte-gated and four-point probe measurements, and Agilent E5270B for the low-temperature transport data that were obtained in a nitrogen-cooled Janis ST-500 cryogenic probe station.

SUPPLEMENTARY MATERIALS

Supplementary material for this article is available at http://advances.sciencemag.org/cgi/content/full/3/9/eaao1558/DC1

fig. S1. Absorption spectrum of the used PbS CQDs in tetrachloroethylene.
fig. S2. Gaussian fits to the measured PL spectra and the fit parameters.
fig. S3. Rutherford backscattering spectra of samples prepared with different amounts of sulfides (see the sample numbers, concentrations, and compositions in table S1).
fig. S4. Temperature dependence of the current extracted from Fig. 3E at +60-V gate bias (highly sulfurized sample, off-state current, high-temperature regime).
fig. S5. Room temperature four-point probe conductivities of nongated films prepared with various sulfide concentrations.
fig. S6. Capacitance of the ion gel between two ITO electrodes for a wide voltage and frequency range.
table S1. Composition obtained from RBS measurements.
table S2. Calculated number of the different atoms in a quantum dot.
table S3. Reported mobilities from the literature measured in PbS FETs.
References (*39*–*41*)

REFERENCES AND NOTES

1. C.-H. M. Chuang, P. R. Brown, V. Bulović, M. G. Bawendi, Improved performance and stability in quantum dot solar cells through band alignment engineering. *Nat. Mater.* **13**, 796–801 (2014).
2. X. Lan, O. Voznyy, F. P. García de Arquer, M. Liu, J. Xu, A. H. Proppe, G. Walters, F. Fan, H. Tan, M. Liu, Z. Yang, S. Hoogland, E. H. Sargent, 10.6% certified colloidal quantum dot solar cells via solvent-polarity-engineered halide passivation. *Nano Lett.* **16**, 4630–4634 (2016).
3. J.-S. Lee, M. V. Kovalenko, J. Huang, D. S. Chung, D. V. Talapin, Band-like transport, high electron mobility and high photoconductivity in all-inorganic nanocrystal arrays. *Nat. Nanotechnol.* **6**, 348–352 (2011).
4. J. Jang, W. Liu, J. S. Son, D. V. Talapin, Temperature-dependent Hall and field-effect mobility in strongly coupled all-inorganic nanocrystal arrays. *Nano Lett.* **14**, 653–662 (2014).
5. T. Chen, K. V. Reich, N. J. Kramer, H. Fu, U. R. Kortshagen, B. I. Shklovskii, Metal–insulator transition in films of doped semiconductor nanocrystals. *Nat. Mater.* **15**, 299–303 (2016).
6. J.-H. Choi, H. Wang, S. J. Oh, T. Paik, P. Sung, J. Sung, X. Ye, T. Zhao, B. T. Diroll, C. B. Murray, C. R. Kagan, Exploiting the colloidal nanocrystal library to construct electronic devices. *Science* **352**, 205–208 (2016).
7. D. Zhitomirsky, M. Furukawa, J. Tang, P. Stadler, S. Hoogland, O. Voznyy, H. Liu, E. H. Sargent, N-type colloidal-quantum-dot solids for photovoltaics. *Adv. Mater.* **24**, 6181–6185 (2012).
8. S. J. Oh, Z. Wang, N. E. Berry, J.-H. Choi, T. Zhao, E. A. Gaulding, T. Paik, Y. Lai, C. B. Murray, C. R. Kagan, Engineering charge injection and charge transport for high performance PbSe nanocrystal thin film devices and circuits. *Nano Lett.* **14**, 6210–6216 (2014).
9. D. M. Balazs, D. N. Dirin, H.-H. Fang, L. Protesescu, G. H. ten Brink, B. J. Kooi, M. V. Kovalenko, M. A. Loi, Counterion-mediated ligand exchange for PbS colloidal quantum dot superlattices. *ACS Nano* **9**, 11951–11959 (2015).
10. E. J. D. Klem, H. Shukla, S. Hinds, D. D. MacNeil, L. Levina, E. H. Sargenta, Impact of dithiol treatment and air annealing on the conductivity, mobility, and hole density in PbS colloidal quantum dot solids. *Appl. Phys. Lett.* **92**, 212105 (2008).
11. D. M. Balazs, M. I. Nugraha, S. Z. Bisri, M. Sytnyk, W. Heiss, M. A. Loi, Reducing charge trapping in PbS colloidal quantum dot solids. *Appl. Phys. Lett.* **104**, 112104 (2014).
12. M. J. Speirs, D. N. Dirin, M. Abdu-Aguye, D. M. Balazs, M. V. Kovalenko, M. A. Loi, Temperature dependent behaviour of lead sulfide quantum dot solar cells and films. *Energy Environ. Sci.* **9**, 2916–2924 (2016).
13. A. Stavrinadis, G. Konstantatos, Strategies for the controlled electronic doping of colloidal quantum dot solids. *ChemPhysChem* **17**, 632–644 (2016).
14. R. S. Allgaier, W. W. Scanlon, Mobility of electrons and holes in PbS, PbSe, and PbTe between room temperature and 4.2°K. *Phys. Rev.* **111**, 1029–1037 (1958).
15. D. Kim, D.-H. Kim, J.-H. Lee, J. C. Grossman, Impact of stoichiometry on the electronic structure of PbS quantum dots. *Phys. Rev. Lett.* **110**, 196802 (2013).
16. S. J. Oh, N. E. Berry, J.-H. Choi, E. A. Gaulding, H. Lin, T. Paik, B. T. Diroll, S. Muramoto, C. B. Murray, C. R. Kagan, Designing high-performance PbS and PbSe nanocrystal electronic devices through stepwise, post-synthesis, colloidal atomic layer deposition. *Nano Lett.* **14**, 1559–1566 (2014).
17. S. J. Oh, N. E. Berry, J.-H. Choi, E. A. Gaulding, T. Paik, S.-H. Hong, C. B. Murray, C. R. Kagan, Stoichiometric control of lead chalcogenide nanocrystal solids to enhance their electronic and optoelectronic device performance. *ACS Nano* **7**, 2413–2421 (2013).
18. A. Stavrinadis, D. So, G. Konstantatos, Low-temperature, solution-based sulfurization and necking of PbS CQD films. *J. Phys. Chem. C* **120**, 20315–20322 (2016).
19. W. J. Baumgardner, K. Whitham, T. Hanrath, Confined-but-connected quantum solids via controlled ligand displacement. *Nano Lett.* **13**, 3225–3231 (2013).
20. I. Moreels, K. Lambert, D. Smeets, D. De Muynck, T. Nollet, J. C. Martins, F. Vanhaecke, A. Vantomme, C. Delerue, G. Allan, Z. Hens, Size-dependent optical properties of colloidal PbS quantum dots. *ACS Nano* **3**, 3023–3030 (2009).
21. W. W. Scanlon, Intrinsic optical absorption and the radiative recombination lifetime in PbS. *Phys. Rev.* **109**, 47–50 (1958).
22. Y. Saito, Y. Iwasa, Ambipolar insulator-to-metal transition in black phosphorus by ionic-liquid gating. *ACS Nano* **9**, 3192–3198 (2015).
23. H. Okimoto, T. Takenobu, K. Yanagi, Y. Miyata, H. Shimotani, H. Kataura, Y. Iwasa, Tunable carbon nanotube thin-film transistors produced exclusively via inkjet printing. *Adv. Mater.* **22**, 3981–3986 (2010).
24. K. Ueno, S. Nakamura, H. Shimotani, A. Ohtomo, N. Kimura, T. Nojima, H. Aoki, Y. Iwasa, M. Kawasaki, Electric-field-induced superconductivity in an insulator. *Nat. Mater.* **7**, 855–858 (2008).
25. M. S. Kang, J. Lee, D. J. Norris, C. D. Frisbie, High carrier densities achieved at low voltages in ambipolar PbSe nanocrystal thin-film transistors. *Nano Lett.* **9**, 3848–3852 (2009).
26. S. Z. Bisri, C. Piliego, M. Yarema, W. Heiss, M. A. Loi, Low driving voltage and high mobility ambipolar field-effect transistors with PbS colloidal nanocrystals. *Adv. Mater.* **25**, 4309–4314 (2013).
27. D. Braga, I. Gutiérrez Lezama, H. Berger, A. F. Morpurgo, Quantitative determination of the band gap of WS_2 with ambipolar ionic liquid-gated transistors. *Nano Lett.* **12**, 5218–5223 (2012).
28. S. Z. Bisri, E. Degoli, N. Spallanzani, G. Krishnan, B. J. Kooi, C. Ghica, M. Yarema, W. Heiss, O. Pulci, S. Ossicini, M. A. Loi, Determination of the electronic energy levels of colloidal nanocrystals using field-effect transistors and ab-initio calculations. *Adv. Mater.* **26**, 5639–5645 (2014).
29. A. Sahu, M. S. Kang, A. Kompch, C. Notthoff, A. W. Wills, D. Deng, M. Winterer, C. D. Frisbie, D. J. Norris, Electronic impurity doping in CdSe nanocrystals. *Nano Lett.* **12**, 2587–2594 (2012).
30. J. Fuller, A. C. Breda, R. T. Carlin, Ionic liquid-polymer gel electrolytes. *J. Electrochem. Soc.* **144**, L67–L70 (1997).
31. E. M. Miller, D. M. Kroupa, J. Zhang, P. Schulz, A. R. Marshall, A. Kahn, S. Lany, J. M. Luther, M. C. Beard, C. L. Perkins, J. van de Lagemaat, Revisiting the valence and conduction band size dependence of PbS quantum dot thin films. *ACS Nano* **10**, 3302–3311 (2016).
32. O. Madelung, U. Rössler, M. Schulz, *Non-Tetrahedrally Bonded Elements and Binary Compounds I* (Springer Verlag, 1998), pp. 1–5.
33. P. R. Brown, D. Kim, R. R. Lunt, N. Zhao, M. G. Bawendi, J. C. Grossman, V. Bulović, Energy level modification in lead sulfide quantum dot thin films through ligand exchange. *ACS Nano* **8**, 5863–5872 (2014).
34. O. Voznyy, D. Zhitomirsky, P. Stadler, Z. Ning, S. Hoogland, E. H. Sargent, A charge-orbital balance picture of doping in colloidal quantum dot solids. *ACS Nano* **6**, 8448–8455 (2012).
35. M. J. Speirs, D. M. Balazs, D. N. Dirin, M. V. Kovalenko, M. A. Loi, Increased efficiency in pn-junction PbS QD solar cells via NaHS treatment of the p-type layer. *Appl. Phys. Lett.* **110**, 103904 (2017).
36. M. A. Hines, G. D. Scholes, Colloidal PbS nanocrystals with size-tunable near-infrared emission: Observation of post-synthesis self-narrowing of the particle size distribution. *Adv. Mater.* **15**, 1844–1849 (2003).
37. L. R. Doolittle, A semiautomatic algorithm for Rutherford backscattering analysis. *Nucl. Instrum. Methods Phys. Res. B* **15**, 227–231 (1986).
38. K. H. Lee, M. S. Kang, S. Zhang, Y. Gu, T. P. Lodge, C. D. Frisbie, "Cut and Stick" rubbery ion gels as high capacitance gate dielectrics. *Adv. Mater.* **24**, 4457–4462 (2012).
39. A. G. Shulga, L. Piveteau, S. Z. Bisri, M. V. Kovalenko, M. A. Loi, Double gate PbS quantum dot field-effect transistors for tuneable electrical characteristics. *Adv. Electron. Mater.* **2**, 1500467 (2016).
40. T. P. Osedach, N. Zhao, T. L. Andrew, P. R. Brown, D. D. Wanger, D. B. Strasfeld, L.-Y. Chang, M. G. Bawendi, V. Bulović, Bias-stress effect in 1,2-ethanedithiol-treated PbS quantum dot field-effect transistors. *ACS Nano* **6**, 3121–3127 (2012).
41. W.-k. Koh, S. R. Saudari, A. T. Fafarman, C. R. Kagan, C. B. Murray, Thiocyanate-capped PbS nanocubes: Ambipolar transport enables quantum dot based circuits on a flexible substrate. *Nano Lett.* **11**, 4764–4767 (2011).

Acknowledgments: We thank A. Kamp and T. Zaharia for technical assistance, J. Momand and B. Kooi for assistance with TEM, and S. Bisri and P. Guyot-Sionnest for discussions on electrolyte-gated transistors. **Funding:** This work was supported by the European Research Council (ERC Starting Grant "Hy-SPOD" No. 306983 to M.A.L., D.M.B., and H.-H.F.), the European Union through the FP7 (ERC Starting Grant NANOSOLID, GA No. 306733 to M.V.K. and D.N.D.), and the Swiss Federal Commission for Technology and Innovation (CTI-No. 18614.1 PFNM-NM).
Author contributions: D.M.B. and M.A.L. conceived the project. D.N.D. synthesized the nanocrystals. D.M.B. and K.I.B. performed the recipe optimization and the transport measurements. D.M.B. prepared all other samples and conducted the TEM and UV-vis characterization and the related data analysis. H.-H.F. performed the PL experiments. M.D. obtained and analyzed the RBS data. M.V.K. and M.A.L. led the project. D.M.B. wrote the manuscript with contributions from all authors. **Competing interests:** The authors declare that they have no competing interests. **Data and materials availability:** All data needed to evaluate the conclusions in the paper are present in the paper and/or the Supplementary Materials. Additional data related to this paper may be requested from the authors.

Submitted 20 June 2017
Accepted 7 September 2017
Published 29 September 2017
10.1126/sciadv.aao1558

Citation: D. M. Balazs, K. I. Bijlsma, H.-H. Fang, D. N. Dirin, M. Döbeli, M. V. Kovalenko, M. A. Loi, Stoichiometric control of the density of states in PbS colloidal quantum dot solids. *Sci. Adv.* **3**, eaao1558 (2017).

ScienceAdvances

Stoichiometric control of the density of states in PbS colloidal quantum dot solids

Daniel M. Balazs, Klaas I. Bijlsma, Hong-Hua Fang, Dmitry N. Dirin, Max Döbeli, Maksym V. Kovalenko and Maria A. Loi

Sci Adv **3** (9), eaao1558.
DOI: 10.1126/sciadv.aao1558